Materials Research Letters

ISSN: (Print) (Online) Journal homepage: www.tandfonline.com/journals/tmrl20

Exploring unusual Lüders deformation in ultrafine-grained high-Mn austenitic steel

Sukyoung Hwang, Hirokazu Kato, Kazuho Okada, Myeong-heom Park, Avala Lavakumar, Reza Gholizadeh, Hiroki Adachi, Masugu Sato & Nobuhiro Tsuji

To cite this article: Sukyoung Hwang, Hirokazu Kato, Kazuho Okada, Myeong-heom Park, Avala Lavakumar, Reza Gholizadeh, Hiroki Adachi, Masugu Sato & Nobuhiro Tsuji (2024) Exploring unusual Lüders deformation in ultrafine-grained high-Mn austenitic steel, Materials Research Letters, 12:8, 571-579, DOI: 10.1080/21663831.2024.2359611

To link to this article: https://doi.org/10.1080/21663831.2024.2359611

MATER. RES. LETT.
2024, VOL. 12, NO. 8, 571–579
https://doi.org/10.1080/21663831.2024.2359611

MATERIALS RESEARCH LETTERS
Taylor & Francis
Taylor & Francis Group

ORIGINAL REPORTS

Exploring unusual Lüders deformation in ultrafine-grained high-Mn austenitic steel

Sukyoung Hwang[a], Hirokazu Kato[a], Kazuho Okada[a,b], Myeong-heom Park[a], Avala Lavakumar[a,c], Reza Gholizadeh[a], Hiroki Adachi[d], Masugu Sato[e] and Nobuhiro Tsuji[a]

[a]Department of Materials Science and Engineering, Kyoto University, Kyoto, Japan; [b]Research Center for Structural Materials, National Institute for Materials Science (NIMS), Tsukuba, Japan; [c]Department of Metallurgical and Materials Engineering, Indian Institute of Technology Ropar, Punjab, India; [d]Department of Materials and Synchrotron Radiation Engineering, Graduate School of Engineering, University of Hyogo, Himeji, Japan; [e]Japan Synchrotron Radiation Research Institute (JARSI), Sayo-gun, Hyogo, Japan

ABSTRACT

Ultrafine-grained (UFG) high-Mn austenitic steel exhibited unusual discontinuous yielding on its stress-strain curve, characterized by a yield drop followed by a stress plateau, indicative of Lüders deformation. Utilizing the digital image correlation (DIC) technique, a strain-localized region known as a Lüders band was observed to propagate during Lüders deformation. Following microstructural observations using state-of-the-art techniques such as *in-situ* synchrotron XRD measurement during the tensile test and *ex-situ* S/TEM and SEM-ECCI, dislocation multiplication, rather than twinning, was theoretically identified as the primary deformation mechanism responsible for the unusual Lüders deformation in UFG high-Mn austenitic steel.

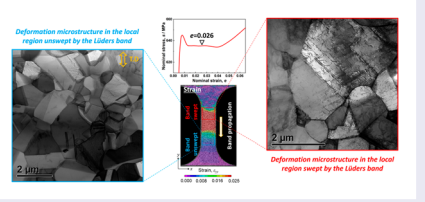

ARTICLE HISTORY
Received 18 March 2024

KEYWORDS
High-Mn austenitic steel; yield point; Lüders deformation; ultrafine grains; TWIP effect

1. Introduction

The mechanical behavior of polycrystalline materials, including yielding, strain hardening and fracture, is closely associated with the inhomogeneous deformation occurring at different scales. Lüders deformation is a typical example of inhomogeneous deformation occurring at the macroscale, characterized by the formation, propagation and annihilation of a strain-localized region known as a Lüders band. This phenomenon has been frequently observed in coarse-grained low-carbon ferritic steel with a BCC structure [1,2]. Such Lüders banding is a process of overcoming plastic instability condition, manifesting as discontinuous yielding followed by a stress plateau on the stress-strain curve [3]. Interestingly, ultrafine-grained (UFG) materials also frequently exhibit Lüders deformation, irrespective of their crystal structure and the presence of solute atoms [4–10]. In UFG pure metals, such as copper [4], aluminium [5], and IF steel [5], strain localization within the Lüders band is attributed to dislocation multiplication, considering the reduced mean free path for dislocation glide in ultrafine grains. On the other hand, in advanced high-strength steels (AHSS) such as TRIP (Transformation-induced plasticity) and TWIP (Twinning-induced plasticity) steels, additional strain-hardening mechanisms can help overcome macroscopic necking and facilitate the propagation of a strain-localized region, thereby achieving remarkable mechanical properties that combine both high strength and ductility [6,8,11–14]. UFG TRIP steel demonstrated enhanced strain hardening due to the high internal stress of deformation-induced martensite, which facilitated stable propagation of the Lüders band [6]. UFG TWIP steel

CONTACT Sukyoung Hwang hwang.sukyoung.8p@kyoto-u.ac.jp Department of Materials Science and Engineering, Kyoto University, Yoshida-honmachi, Sakyo-ku, Kyoto 606, Japan

Supplemental data for this article can be accessed online at https://doi.org/10.1080/21663831.2024.2359611.

exhibited unusual discontinuous yielding despite its FCC structure [8,11–14]. Bai et al. [8] reported that such unexpected discontinuous yielding in Fe-31Mn-3Al-3Si steel was closely related with the promotion of deformation twinning, due to the scarce availability of free dislocations in ultrafine grains, and it played a critical role in enhancing the strain hardening through the subdivision of prior austenite grains (the so-called dynamic Hall-Petch effect). While the achievements have established a qualitative relationship between deformation twinning and discontinuous yielding (or Lüders deformation), the quantitative contribution of twinning to Lüders deformation in high-Mn steel remains unclear. The current study aims to explore the origin of Lüders deformation in UFG high-Mn steel across multiple scales. The macroscopic Lüders deformation in UFG high-Mn steel was quantified using digital image correlation (DIC) technique applied during tensile deformation, and it was correlated with microstructural changes characterized by state-of-the-art synchrotron XRD measurement, S/TEM, and SEM-ECCI.

2. Materials and methods

High-Mn steel with a composition of Fe-31Mn-3Al-3Si (wt. %) was used in this study. The as-received bulk plate underwent multi-pass cold-rolling, achieving a 92% reduction in thickness. An UFG specimen with a mean grain size of 0.65 µm was fabricated by annealing the cold-rolled sheet at 700°C for 300 s, followed by water quenching. Similarly, a fine-grained (FG) specimen with a mean grain size of 4.5 µm was fabricated by annealing at 850°C for 600 s, serving as a reference material that shows continuous yielding. The microstructure was observed using a field-emission scanning electron microscope (FE-SEM: JEOL JSM-7800F) equipped with a backscattered electron (BSE) detector at an accelerating voltage of 15 kV. The preparation of specimens for SEM-BSE, SEM-ECCI, and S/TEM observations is detailed in the Supplementary Material. The mean grain size was measured by a line intercept method on SEM-BSE image, counting high-angle grain boundaries and annealing twin boundaries. Tensile tests were performed at room temperature at constant rate of elongation (initial strain rate of $8.3 \times 10^{-4}\,s^{-1}$) using sheet-type tensile specimens, which are described in the Supplementary Material (Figure S1). Small speckle patterns were applied to the white-painted background of the tensile specimens, and DIC images were captured at five FPS during the tensile test to evaluate both global and local strain distribution using Vic-2D software.

In-situ synchrotron XRD measurement with the beam position fixed was performed with the DIC technique during tensile deformation at the beamline of BL46 XU at SPring-8. The setup and conditions for the experiment are detailed in Supplementary Material (Figure S2). The first five diffraction peaks were analyzed using the convolutional multiple whole profile (CMWP) fitting method [15,16]. Detailed fitting results (Figure S3), along with calculation of dislocation density and stacking fault probability, can be found in the Supplementary Material. *Ex-situ* observations of deformation microstructures within and beyond the Lüders band were conducted using scanning transmission electron microscopy (S/TEM: JEOL JEM-2100F) operated at 200 kV, and the SEM-electron channeling contrast imaging (ECCI) technique at an accelerating voltage of 15 kV. The area fraction of deformation twins was quantified on the SEM-ECC images using GIMP 2.10 software, as described in the Supplementary Material (Figure S4).

3. Results and discussion

Figure 1(a and b) show the SEM-BSE images of the UFG and FG specimens, respectively. Both specimens exhibited a fully recrystallized microstructure containing many annealing twins. The UFG and FG specimens had mean grain sizes of 0.65 and 4.5 µm, respectively. Both specimens showed weak textures, with details provided in the Supplementary Material (Figure S5). Figure 1(c) shows the nominal stress-strain curves of the UFG and FG specimens. The FG specimen exhibited a yield strength (0.2% proof stress) of 300 MPa, a tensile strength of 632 MPa, and a total elongation of 66%. The UFG specimen demonstrated a much higher yield strength of 645 MPa (upper yield strength), tensile strength of 817 MPa, and a total elongation of 60%. Such enhancement of mechanical properties in the UFG specimen has been attributed to a remarkable increase in deformation twinning [8,17]. It should also be noted that the yielding behavior differed distinctly between the UFG and FG specimens. The UFG specimen showed discontinuous yielding characterized by a yield drop and subsequent stress plateau, i.e. Lüders deformation, while the FG specimen exhibited continuous yielding behavior. The yield drop of 11 MPa was caused by local yielding, and its propagation manifested as a Lüders strain of 0.030 (3.0%) during the stress plateau. DIC movies illustrating the changes in local strain rate (Movie 1) and local strain distributions (Movie 2) during Lüders deformation are included as Supplementary Material, capturing the formation, propagation and annihilation of the Lüders band distinctly.

The *in-situ* synchrotron XRD measurement and DIC analysis were performed simultaneously during the tensile test, and the results are shown in Figure 2. Figure 2(a)

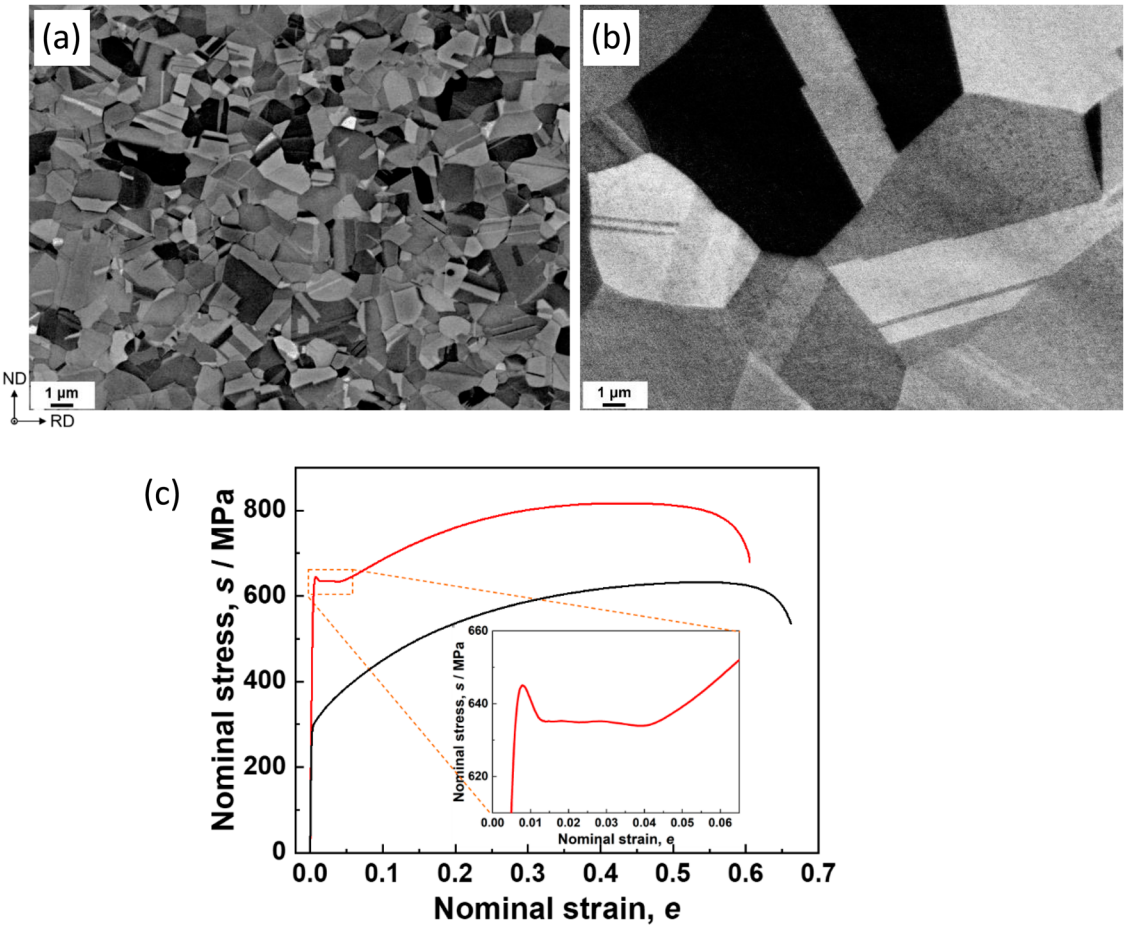

Figure 1. SEM-BSE images of the Fe-31Mn-3Al-3Si steels with mean grain sizes of (a) 0.65 μm and (b) 4.5 μm, observed from the transverse direction (TD) of the rolled sheet. (c) Nominal stress-strain curves of the UFG and FG specimens.

shows the DIC strain-rate maps during the Lüders deformation, showing the front of the Lüders band, characterized by a higher local strain rate, propagating through the tensile specimen from (1) to (5). Hereafter, the front of the Lüders band will be referred to as the 'Lüders front', and the process from (1) to (5) as 'Lüders banding'. Changes in XRD profiles from (1) to (5) are shown in different colors in Figure 2(b). During such Lüders banding, diffraction peaks shifted and broadened. For detailed investigation, five diffraction peaks at moments from (2) to (4), during which the Lüders front was propagating near the beam position, are enlarged in Figure 2(c–g). All five diffraction peaks broadened as the Lüders front passed through the beam position, indicating that defects were introduced in the local area of the beam position. Interestingly, however, the direction and extent of peak shifts were complex and differed for each peak, as indicated by arrows in the figures. The real-time changes in peak shifts for five diffraction peaks, along with the global tensile stress during the early stage of deformation, are presented in Supplementary Material (Figure S6). Normally, yielding behavior relaxes elastic strain (and consequently stress), causing diffraction peaks to shift to higher angles irrespective of the peaks. On the other hand, complex peak shifts observed in this study are attributed to the generation of stacking faults, which shift diffraction peaks either to higher or lower angles depending on the Miller indices (hkl) of the crystal plane [18]. The CWMP method was employed to effectively evaluate both dislocation density and stacking fault probability [19,20]. Figure 2(h) shows changes in dislocation density as the Lüders front passed through the beam position. From (1) to (2), corresponding to the period before the Lüders front reached the beam position, dislocation density rarely changed. However, from (2) to (4), during which the Lüders front passed through the beam position, dislocation density significantly increased. It is noticeable that the dislocation density increased significantly, by approximately 300 times, from 4.7×10^{12} to $1.4 \times 10^{15} m^{-2}$. From (4) to (5), after the Lüders front passed beyond the beam position, dislocation density returned to barely changing. Figure 2(i) shows changes in stacking fault probability (SFP) from (1) to (5). SFP quantifies the chance of forming a stacking fault in the FCC

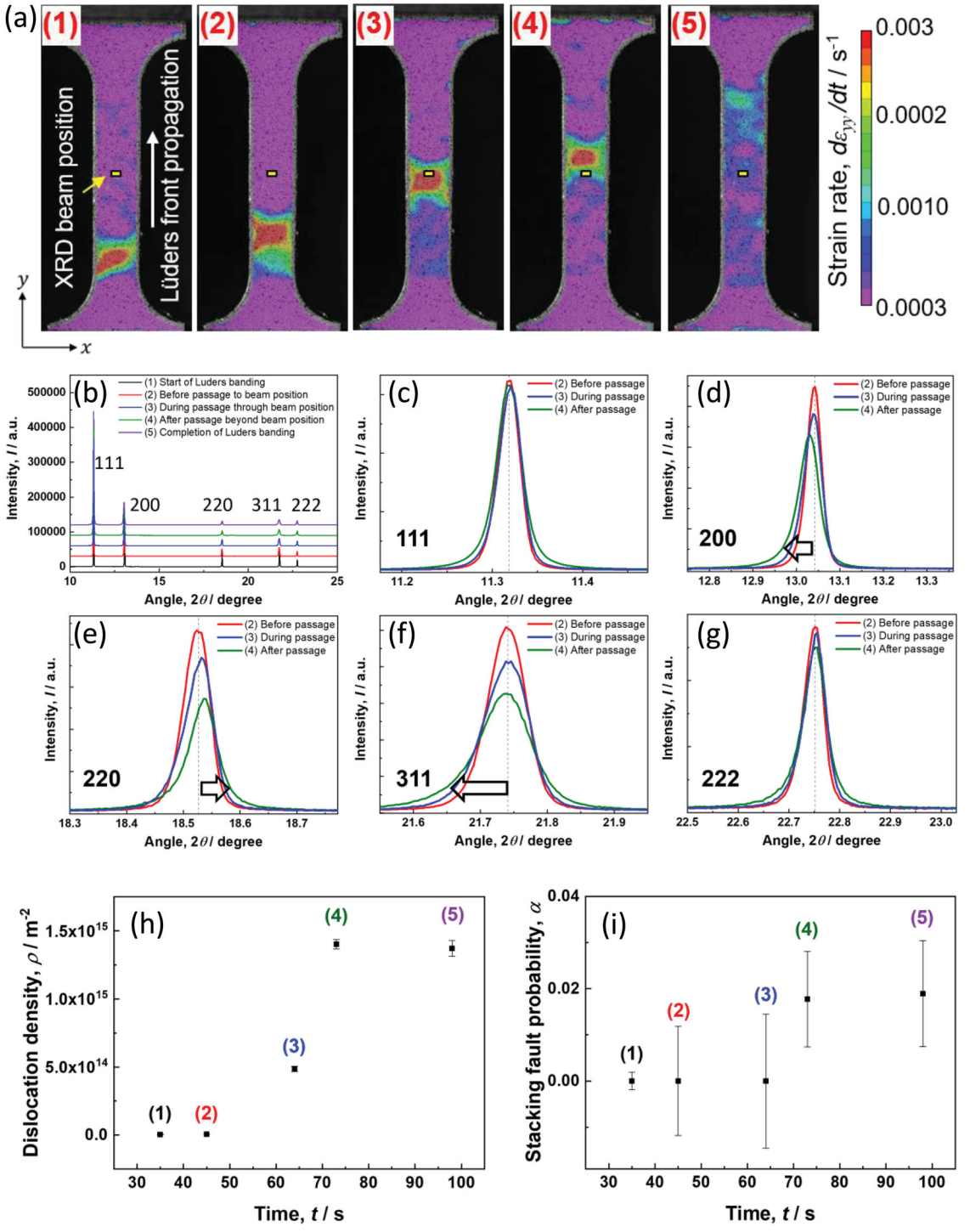

Figure 2. (a) DIC strain-rate maps showing the Lüders banding observed in the UFG specimen. The yellow point in each DIC image indicates the position irradiated by incident X-ray beam. (b) The entire angular diffraction pattern during Lüders banding ((1) to (5)), and (c-g) enlarged five diffractions peaks with a black dashed line in each figure indicating the peak center at (2). Changes in (h) dislocation density and (i) stacking fault probability, including error bars, during Lüders banding.

matrix [20]. Similar to the change in dislocation density, before the Lüders front reached the beam position (from (1) to (2)), SFP remained unchanged. During its passage through the beam position (at (3)), there was a notable increase in SFP, but it reached only 1.8% (at (4)). Subsequently, SFP rarely changed after its passage (from (4) to (5)). The results suggest that dislocation multiplication contribute more to Lüders strain than stacking faults

(or leading partial dislocations), which had a low probability (1.8%) and produced smaller plastic strain due to the smaller Burgers vector of a leading partial dislocation than that of a perfect dislocation [21].

For direct observation of deformation microstructures associated with Lüders banding, S/TEM observation was conducted. As shown in Figure 3(a), the tensile test was interrupted at a global strain of $e = 0.026$, during which strain locally accumulated to 0.039 as the Lüders band swept the right half of the gage part. Subsequently, S/TEM specimens were prepared for two distinct groups: one where the Lüders band had not swept and the other where the Lüders band had already swept. To capture the overall trend, deformation microstructures in broad areas,

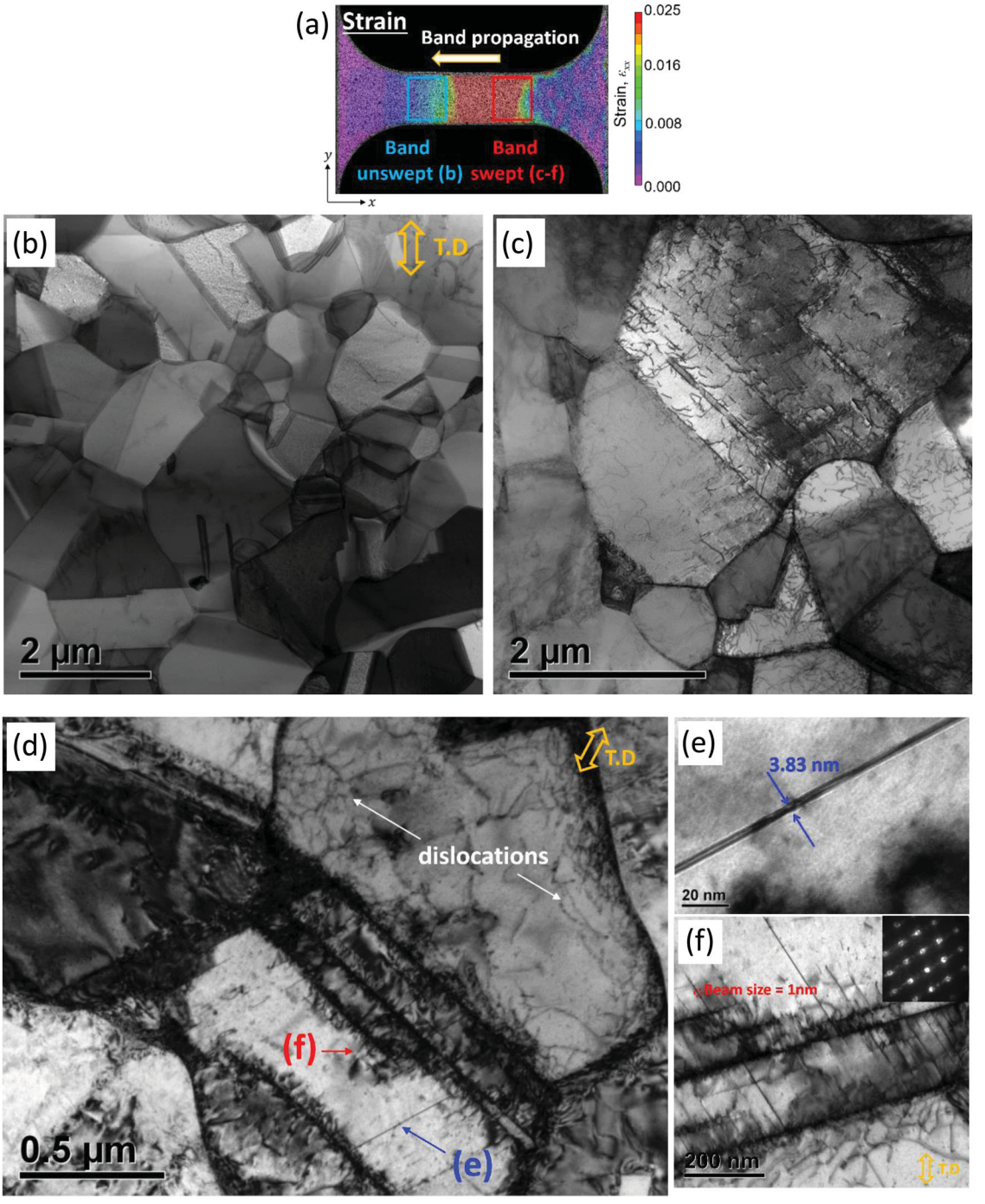

Figure 3. (a) DIC local strain map of the UFG specimen at unloading point, and STEM images in regions of (b) the band unswept and (c) the band swept. (d) Deformation microstructure in the region swept by the band, containing (e) a nanotwin and (f) stacking faults, with an inset of the NBD pattern showing streaks. Note that the image in (f) appears flipped compared to Figure 3(d) due to the inverted specimen setting. Tensile direction (TD) is indicated in the figures.

both beyond and within the Lüders band, were observed in STEM mode. The corresponding STEM images are shown in Figure 3(b and c), respectively. The deformation microstructures were clearly different in relation to the Lüders banding. The local region where the Lüders band had not swept included a small number of defects (Figure 3(b)), whereas the local region where the Lüders band had swept contained a large number of defects across several grains (Figure 3(c)). For a detailed investigation, a region where Lüders band had swept is observed and shown in Figure 3(d). In addition to many dislocations, some nanotwins were also observed, with one of them enlarged in Figure 3(e). It is noteworthy that deformation twins are few in number even within the Lüders band. As shown in Figure 3(f), many thin plates, each with a thickness of less than 1 nm, formed along the grain boundary (or annealing twin boundary). Using nano beam diffraction (NBD) in STEM mode, these thin plates were identified as possibly being stacking faults, as evidenced by the streaks perpendicular to the stacking faults in the NBD pattern.

To quantify the area fraction of deformation twins across a broader area, the SEM-ECCI technique was employed, and the results are shown in Figure 4. In Figure 4(a), at a global strain of $e = 0.023$, the local strain in the region swept by the Lüders band was 0.0413. Similar to the S/TEM observations, the SEM-ECCI observations were categorized into three groups: one group where the Lüders band had not swept (G1), another where the band was sweeping (G2), and the other where the Lüders band had already swept (G3). As shown in the SEM-ECC images in Figure 4(b–d), in the local region swept by the Lüders band (G3), there was a noticeable increase in deformation twins, as well as dislocations and stacking faults, compared to the unswept region (G1). The area fractions of deformation twins in G1, G2, and G3 are shown in Figure 4(e), together with the local strain distribution along the red line across the gage part. In each group, approximately 30 grains were observed for the precise quantification of the area fraction of deformation twins. The area fraction of deformation twins (f_{twin}) increased from 0.08% ($f_{\text{twin}}^{\text{G1}}$) to 0.18% ($f_{\text{twin}}^{\text{G2}}$) and then to 0.39% ($f_{\text{twin}}^{\text{G3}}$), as the local strain ($\varepsilon_{xx}$) increased from 0.0046 ($\varepsilon_{xx}^{\text{G1}}$) to 0.0219 ($\varepsilon_{xx}^{\text{G2}}$) and then to 0.0391 ($\varepsilon_{xx}^{\text{G3}}$) due to local Lüders banding. However, it is noteworthy that the area fraction of deformation twins remained as low as 0.39% even within the Lüders band ($f_{\text{twin}}^{\text{G3}}$).

Finally, the tensile strain resulting from twinning was theoretically quantified to evaluate its contribution to the macroscopic Lüders strain ($\varepsilon_{xx}^{\text{G3}}$). Figure 5 schematically describes twinning in an FCC matrix.

In the schematic, the leading partial dislocations glided on every (111) layer, with their Burgers vector ($\vec{b}_{\text{LP}}$), shifting atoms from their original positions (hollow circles in the figure) to new positions (solid circles). This process shears (111) layers in the twinned region toward the slip direction of the leading partial dislocation, with the shear angle of θ. Thus, the shear strain generated by twinning (γ_{twin}) is calculated as follow:

$$\gamma_{\text{twin}} = \tan\theta = \frac{|\vec{b}_{\text{LP}}|}{d_{(111)}} \tag{1}$$

where θ is the shear angle, $|\vec{b}_{\text{LP}}|$ is the magnitude of the Burgers vector of the leading partial dislocation, and $d_{(111)}$ is the interplanar distance of the (111) planes. However, the shear strain calculated in Equation (1) must be converted to tensile strain to assess the contribution of twinning to the macroscopic Lüders strain ($\varepsilon_{xx}^{\text{G3}}$), while also considering the effect of crystallographic orientation. In the Taylor model for a uniaxial tensile test, the tensile strain in a unit volume is expressed as:

$$\varepsilon_{xx} = \frac{1}{M} \times \sum \gamma \tag{2}$$

where ε_{xx} is tensile strain in a unit volume, $\sum \gamma$ is the sum of shear strain on each slip (or twinning) plane within a unit volume, and M is the Taylor factor. The Taylor factor for FCC material with a random texture is known to be 3.06, and the present material exhibited no strong texture (Figure S5). Assuming that the primary twinning system is mostly activated during Lüders deformation ($\gamma_{\text{twin}} \approx \sum \gamma$), as shown in Figure 3(c–e) and Figure 4(c and d), the consequent tensile strain ($\varepsilon_{\text{twin}}$) attributed to twinning is estimated to be 0.231. As shown in Figure 4(e), the area fraction deformation twins in the Lüders band ($f_{\text{twin}}^{\text{G3}}$) was measured to be 0.0039 (0.39%). Therefore, out of the macroscopic Lüders strain ($\varepsilon_{xx}^{\text{G3}}$), the contribution of twinning to Lüders strain can be calculated as follow:

$$\frac{\varepsilon_{\text{twin}} \times f_{\text{twin}}^{\text{G3}}}{\varepsilon_{xx}^{\text{G3}}} = 0.0230(2.3\%) \tag{3}$$

The small contribution of twinning to the macroscopic Lüders strain suggests that dislocation multiplication, rather than twinning, is the primary deformation mechanism responsible for the Lüders strain in UFG high-Mn steel, as evidenced by the significant increase in dislocation density within the propagating Lüders band (Figure 2(h)). Such Lüders deformation in UFG high-Mn steel shares a fundamental mechanism with that in other conventional UFG materials where dislocation multiplication serves as the principal mechanism. The role of twinning in enhancing local strain hardening, which enables the Lüders band to propagate, was beyond

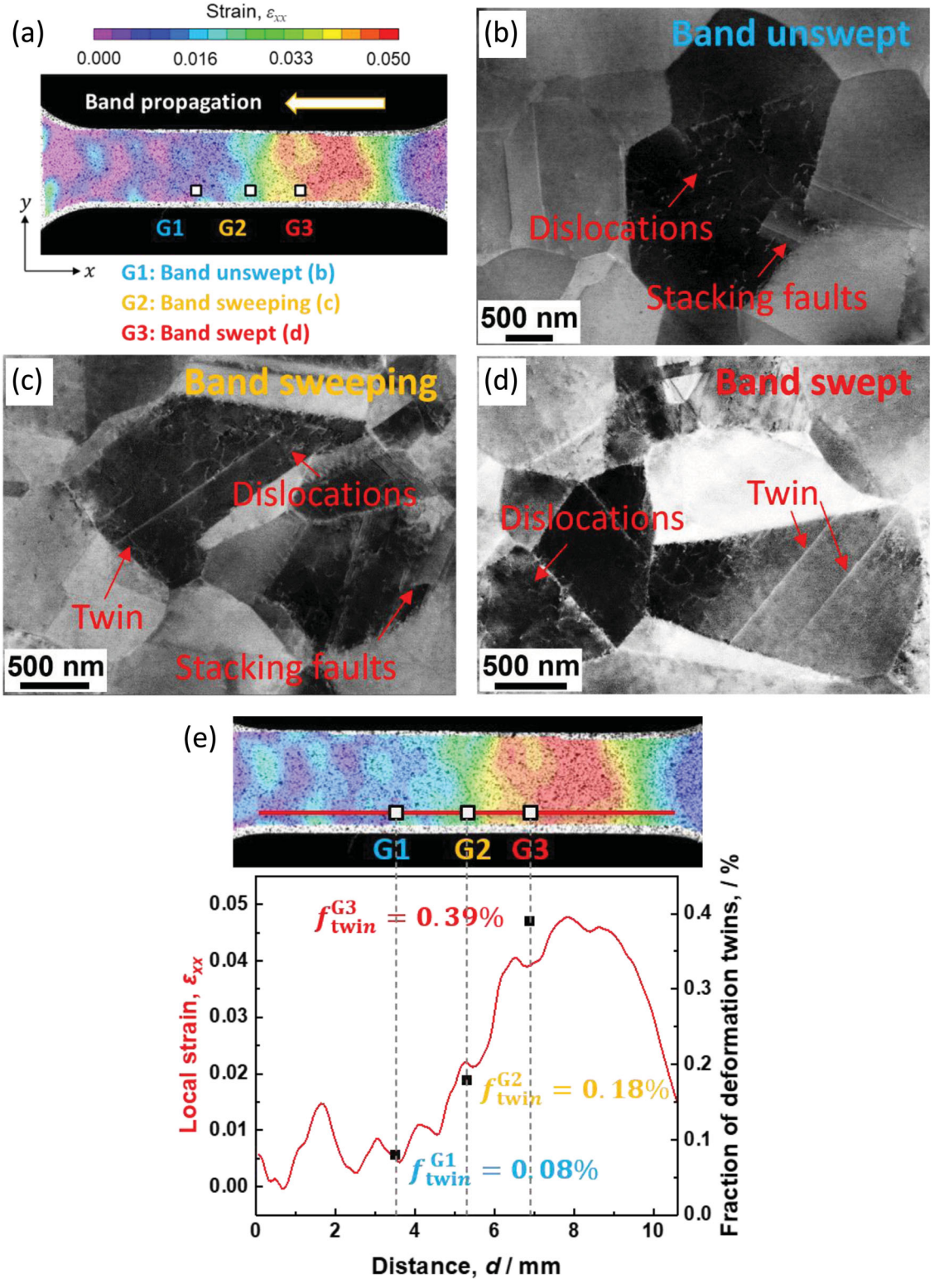

Figure 4. (a) DIC local strain map of the UFG specimen at unloading point. Observations of deformation microstructures were categorized into three groups, G1, G2, and G3, considering Lüders banding. SEM-ECC images showing representative deformation microstructures in regions (b) G1, (c) G2, and (d) G3. (e) Area fractions of deformation twins in regions G1, G2, and G3, plotted with the local strain across the gage part.

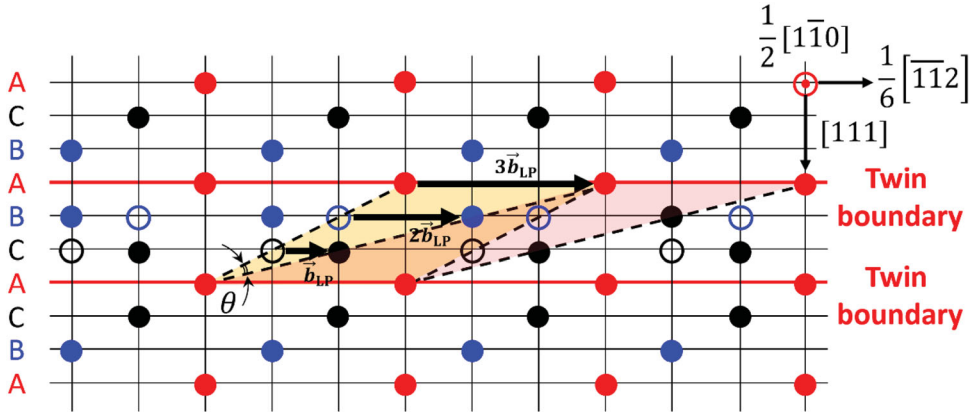

Figure 5. Schematic illustration of shear deformation induced by twinning in an FCC matrix.

the scope of this study, and further research is necessary. Nevertheless, the findings of this study highlight the need for a careful examination of the TWIP effect, often accepted without adequate scrutiny as the underlying mechanism for various mechanical behaviors in high-Mn steels.

4. Conclusions

This research thoroughly explored the origins of unusual Lüders deformation in UFG high-Mn austenitic steel, connecting macroscopic Lüders banding with microscopic deformation mechanism. Utilizing the *in-situ* DIC technique and synchrotron XRD measurement during the tensile test, substantial dislocation multiplication within the propagating Lüders band was observed, while stacking fault probability remained low. Nanosized stacking faults were identified through STEM observation, and the area fraction of deformation twins concerning Lüders banding was extensively quantified using SEM-ECCI technique. The tensile strain given by twinning was theoretically estimated based on the experimental findings, revealing its contribution to macroscopic Lüders strain to be only 2.3%. All results consistently demonstrate that dislocation multiplication, not twinning, was the primary deformation mechanism behind the unusual Lüders deformation in UFG high-Mn austenitic steel.

Acknowledgments

The present study was financially supported by JST CREST (JPMJCR1994), Elements Strategy Initiative for Structural Materials (ESISM, No. JPMXP0112101000), and the Grant-in-Aid for Scientific Research (S) (No. 20H00306, 20K14608, 21K20401, 22K18888, 23H00234, 23K13563 and 23K20037), all through the Ministry of Education, Culture, Sports, Science and Technology (MEXT), Japan. All the supports are gratefully appreciated.

Disclosure statement

No potential conflict of interest was reported by the author(s).

Funding

This work was supported by Japan Society for the Promotion of Science [grant number 20H00306, 22K18888, 23H00234, 23K20037]; Ministry of Education, Culture, Sports, Science and Technology [grant number JPMJCR1994].

References

[1] Fujita H, Miyazaki S. Lüders deformation in polycrystalline iron. Acta Metall. 1978;26(8):1273–1281. doi:10.1016/0001-6160(78)90012-3
[2] Gao S, Shibata A, Chen M, et al. Correlation between continuous/discontinuous yielding and hall–petch slope in high purity iron. Mater Trans. 2014;55:69–72. doi:10.2320/matertrans.MA201326
[3] Schwab R, Ruff V. On the nature of the yield point phenomenon. Acta Mater. 2013;61:1798–1808. doi:10.1016/j.actamat.2012.12.003
[4] Tian YZ, Gao S, Zhao LJ, et al. Remarkable transitions of yield behavior and Lüders deformation in pure Cu by changing grain sizes. Scr Mater. 2018;142:88–91.
[5] Tsuji N, Ito Y, Saito Y, et al. Strength and ductility of ultrafine grained aluminum and iron produced by ARB and annealing. Scr Mater. 2002;47:893–899. doi:10.1016/S1359-6462(02)00282-8
[6] Gao S, Bai Y, Zheng R, et al. Mechanism of huge Lüders-type deformation in ultrafine grained austenitic stainless steel. Scr Mater. 2019;159:28–32.
[7] Xie Y, Liang J, Zhang D, et al. Sustaining strength–ductility synergy of CoCrFeNiMn high entropy alloy by a multilevel heterogeneity associated with nanoparticles. Scr Mater. 2020;187:390–394. doi:10.1016/j.scriptamat.2020.06.054
[8] Bai Y, Kitamura H, Gao S, et al. Unique transition of yielding mechanism and unexpected activation of deformation twinning in ultrafine grained Fe-31Mn-3Al-3Si alloy. Sci Rep [Internet]. 2021;11:15870. doi:10.1038/s41598-021-94800-6

[9] Tsuji N, Ogata S, Inui H, et al. Strategy for managing both high strength and large ductility in structural materials–sequential nucleation of different deformation modes based on a concept of plaston. Scr Mater. 2020;181:35–42. doi:10.1016/j.scriptamat.2020.02.001 Available from: http://www.sciencedirect.com/science/article/pii/S1359646220300579

[10] Zheng R, Bhattacharjee T, Gao S, et al. Change of deformation mechanisms leading to high strength and large ductility in Mg-Zn-Zr-Ca alloy with fully recrystallized ultrafine grained microstructures. Sci Rep. 2019;9:11702. doi:10.1038/s41598-019-48271-5

[11] Jeong S, Kim E, Park J, et al. Effect of grain size on the local deformation behavior associated with the discontinuous yielding in a high Mn austenitic steel. Met Mater Int. 2024. doi:10.1007/s12540-023-01595-4

[12] Chen X, Wang Y, Xiong J, et al. Effect of temperature on the mechanical properties and deformation mechanism of a high Mn steel with composite structure. Front Mater. 2020;7. https://www.frontiersin.org/articles/10.3389fmats.2020.00070.

[13] Hung C-Y, Bai Y, Tsuji N, et al. Grain size altering yielding mechanisms in ultrafine grained high-Mn austenitic steel: advanced TEM investigations. J Mater Sci Technol. 2021;86:192–203. doi:10.1016/j.jmst.2021.01.031 Available from: https://www.sciencedirect.com/science/article/pii/S1005030221001699

[14] Kang S, Jeong S, Ahn Y-S. Effect of discontinuous yielding on the strain hardening behavior of fine-grained twinning-induced plasticity steel. Front Mater [Internet]. 2021: 8. Available from: https://www.frontiersin.org/articles/10.3389fmats.2021.599534

[15] Okada K, Shibata A, Gong W, et al. Effect of hydrogen on evolution of deformation microstructure in low-carbon steel with ferrite microstructure. Acta Mater. 2022;225:117549. doi:10.1016/j.actamat.2021.117549

[16] Ungár T, Dragomir I, Révész Á, et al. The contrast factors of dislocations in cubic crystals: the dislocation model of strain anisotropy in practice. J Appl Crystallogr. 1999;32:992–1002. doi:10.1107/S0021889899009334

[17] Hung C-Y, Shimokawa T, Bai Y, et al. Investigating the dislocation reactions on Σ3111 twin boundary during deformation twin nucleation process in an ultrafine-grained high-manganese steel. Sci Rep. 2021;11:19298. doi:10.1038/s41598-021-98875-z

[18] Paterson MS. X-ray diffraction by face-centered cubic crystals with deformation faults. J Appl Phys. 1952;23:805–811. doi:10.1063/1.1702312

[19] Simm TH. Peak broadening anisotropy and the contrast factor in metal alloys. Crystals (Basel). 2018;8:212.

[20] Balogh L, Ribárik G, Ungár T. Stacking faults and twin boundaries in fcc crystals determined by x-ray diffraction profile analysis. J Appl Phys. 2006;100:023512.

[21] Rae CMF, Matan N, Reed RC. The role of stacking fault shear in the primary creep of [001]-oriented single crystal superalloys at 750°C and 750 MPa. Mater Sci Eng A. 2001;300:125–134. doi:10.1016/S0921-5093(00)01788-3 https://www.sciencedirect.com/science/article/pii/S0921509300017883